Dynamic Observation of Dendritic Quasicrystal Growth upon Laser-Induced Solid-State Transformation

Insung Han,[1] Joseph T. McKeown,[2] Ling Tang,[3] Cai-Zhuang Wang,[4,5] Hadi Parsamehr,[1] Zhucong Xi,[1] Ying-Rui Lu,[6] Matthew J. Kramer,[4] and Ashwin J. Shahani[1,*]

[1]*Department of Materials Science and Engineering, University of Michigan, Ann Arbor, Michigan 48109, USA*
[2]*Materials Science Division, Lawrence Livermore National Laboratory, Livermore, California 94550, USA*
[3]*Department of Applied Physics, College of Science, Zhejiang University of Technology, Hangzhou, 310023, China*
[4]*Ames Laboratory-USDOE, Iowa State University, Ames, Iowa 50011, USA*
[5]*Department of Physics and Astronomy, Iowa State University, Ames, Iowa 50011, USA*
[6]*National Synchrotron Radiation Research Center, Hsinchu 30076, Taiwan*

(Received 23 March 2020; revised 11 July 2020; accepted 16 September 2020; published 6 November 2020)

We report the laser-induced solid-state transformation between a periodic "approximant" and quasicrystal in the Al-Cr system during rapid quenching. Dynamic transmission electron microscopy allows us to capture *in situ* the dendritic growth of the metastable quasicrystals. The formation of dendrites during solid-state transformation is a rare phenomenon, which we attribute to the structural similarity between the two intermetallics. Through *ab initio* molecular dynamics simulations, we identify the dominant structural motif to be a 13-atom icosahedral cluster transcending the phases of matter.

DOI: 10.1103/PhysRevLett.125.195503

Quasicrystals (QCs) have long fascinated physicists owing to their noncrystallographic rotational symmetries and quasiperiodic translational order [1]. Closely related to the QC are "approximant" phases, which share similar structural motifs with QCs yet with periodically stacked atomic layers. Despite their frequent observation in both metallic alloys [2–4] and soft matter structures [5–7], little is known about the growth dynamics of complex intermetallics, including QCs and their approximants. Recent *in situ* studies [8–12] have demonstrated that their solidification behavior is governed by the kinetics of interfacial attachment, the anisotropy of which leads to the presence of facets and polyhedral kinetic shapes. These real-time experiments are typically done under near-equilibrium conditions wherein a liquid is cooled slowly below the liquidus, thereby solidifying in a thermodynamically stable phase. However, the growth mechanisms that control the formation of *metastable* QCs remain an enigma. Such metastable phases are most often encountered under high driving forces in Al-TM alloys (TM: Cr, Mn, among others) [1,13–16]. An experimental assessment of metastable QC formation is inaccessible using conventional approaches as it unfolds too rapidly to discern at small spatial scales.

In this Letter, we show how a metastable icosahedral QC grows dendritically from an approximant phase. We overcome the challenge in observing the growth of QCs far from equilibrium with the aid of dynamic transmission electron microscopy (DTEM) [17–19]. Current state-of-the-art "movie-mode" DTEM [19] enables the recording of a stream of nine images generated by short electron probe pulses following laser irradiation. With this technology, it is possible to capture transient behavior with an unparalleled combination of temporal (∼10 ns) and spatial resolutions (∼10 nm) [20]. These parameters are more than sufficient to visualize the formation of metastable phases [20–25], such as QCs, under superfast pulsed laser-induced cooling rates ($10^5 - 10^7$ K/s). By harnessing these new developments, we provide fresh insights into the growth shapes, growth rates, and growth mechanisms of the metastable QCs, which have a higher degree of phasonic and chemical disorder [26] than ideal QCs [27]. Our results point to the anomalously high mobility of the QC-approximant interfaces, which can sustain diffusional instabilities. We present a cohesive picture of the growth process based on our experimental evidence and supporting molecular dynamics (MD) simulations.

Thin films of composition $Al_{90}Cr_{10}$ and thickness 150 nm were deposited on SiN transmission electron microscopy (TEM) grids via magnetron sputtering. The samples were placed on an *in situ* heating stage in the DTEM and annealed at 340 °C for 5 min, leading to the formation of the $Al_{13}Cr_2$ phase (C2/m) (plus Al). Then, the samples were irradiated by a short pulsed laser with 1064 nm wavelength for 15 ns of exposure time. The laser intensity was tuned to 15.2 μJ to prevent film dewetting and rupture. The microstructural evolution within the heat-affected zone was recorded in DTEM using 50 ns electron probe pulses after a preset delay time.

The local structure of the $Al_{13}Cr_2$ phase before laser irradiation was confirmed by x-ray absorption spectroscopy (XAS). Samples for XAS were prepared in the same manner as for DTEM. The x-ray energy was set above

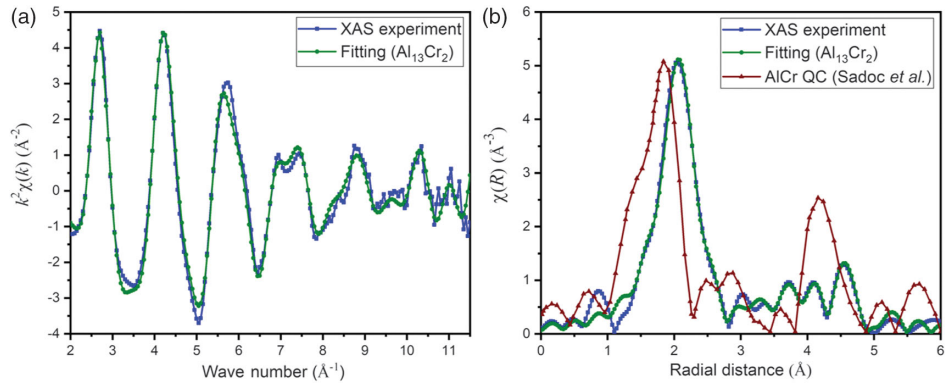

FIG. 1. Comparison of local structure measurements. (a) Experimental EXAFS results of the preirradiated $Al_{90}Cr_{10}$ film and simulated $Al_{13}Cr_2$ structure in the k space. (b) RDFs of the annealed $Al_{90}Cr_{10}$ film, simulated $Al_{13}Cr_2$ structure, and Al-Cr icosahedral QC [40].

the Cr K edge (5989 eV). The IFEFFIT software package [28] was used to analyze the raw XAS spectra in the k space and R space. The data were fitted to simulated $Al_{13}Cr_2$ structure [29].

To further explore the dominant local structures in $Al_{90}Cr_{10}$ that persist after rapid quenching, we performed MD simulations using the neural network interatomic potential developed by deep machine learning [30–32]. This approach describes a structure of liquid $Al_{90}Cr_{10}$ that is compatible with the results from *ab initio* MD calculations. Local structural order in the quenched liquid is analyzed by the cluster alignment analysis method [33] (see the Supplemental Material [34] for more details).

Figure 1(a) presents the extended x-ray absorption fine structure (EXAFS) region of the XAS spectrum of the preirradiated $Al_{90}Cr_{10}$ film and simulated EXAFS results from the approximant $Al_{13}Cr_2$ structure [29] in the k space. The agreement between the experimental and simulated EXAFS spectra and radial distribution functions (RDFs) in Fig. 1(a),(b) indicates that the dominant crystal structure before laser irradiation is $Al_{13}Cr_2$ and not an Al-Cr QC [40]. According to the RDFs shown in Fig. 1(b), the adjacent atomic structures around a Cr atom in the latter are more closely packed than in the former. The structural relationship between the two phases will be elaborated upon later (see below).

We captured via DTEM the microstructural evolution in an $Al_{13}Cr_2$ thin film following laser irradiation. The temperature profile of our sample (simulated via COMSOL in Fig. S1 in the Supplemental Material [34], which is based on the assumptions in [24] and parameters from [41,42]) suggests that the maximum temperature attained is below 600 °C, which is not sufficient to melt the sample (note the liquidus temperature of $Al_{90}Cr_{10}$ is 930 °C). Thus, the ensuing phase transformation occurs entirely in the *solid state*.

The growth sequence of single representative precipitate embedded in an approximant matrix is shown in Fig. 2(a) after image processing (see also Fig. S2 in the Supplemental Material [34]). Following an initial incubation period, we were able to observe the growth and morphological evolution of the precipitate from a sphere to a dendrite. The latter transition occurred at some point between (ii) and (v) in Fig. 2(a). No facets were observed at the resolution of the images. Eventually the growth process terminates due to reduced driving forces [43] and/or solid diffusivities [44]. (The temperature-dependent Cr supersaturation and diffusion are dealt with further in the Supplemental Material [34].) When these same samples were irradiated with a single pulse laser for a second time [Fig. 2(b)], QC growth occurred almost instantly. This is because the preexisting precipitates or "seeds" serve as templates for QC growth. This result is further confirmation that the phase transformation proceeds entirely in the solid state since the QC liquidus is underneath the approximant liquidus [15]. We measure growth velocities of ~0.01 m/s [see Fig. 2(c)], whether or not the sample contains the seeds. However, the incubation times, determined by extrapolating the growth curves in Fig. 2(c) to the zero-radius axis, are substantially different: ~0 μs with seeds vs ~170 μs without seeds.

TEM revealed that the fully grown crystals are indeed icosahedral QCs, as demonstrated by the fivefold selected area electron diffraction pattern [see Fig. 2(d)]. Corresponding energy dispersive spectroscopy analysis showed that these QCs are enriched in Cr and that they reject Al into the interdendritic regions during precipitation (see Fig. S3 in the Supplemental Material [34]). Thus, QC growth is rate-limited by diffusion and not collision [45] since we can find solute partitioning. The average QC grain size was approximately 2 μm (see Fig. S4 in the Supplemental Material [34]).

In general, a number of preconditions must be met in order for precipitates to grow dendritically. These include (i) an isotropic precipitate-matrix interfacial energy, (ii) low diffusivity within the growing precipitate, (iii) a low "mismatch" between the precipitate and matrix, and (iv) a low precipitate nucleation density [44,46,47]. All of these

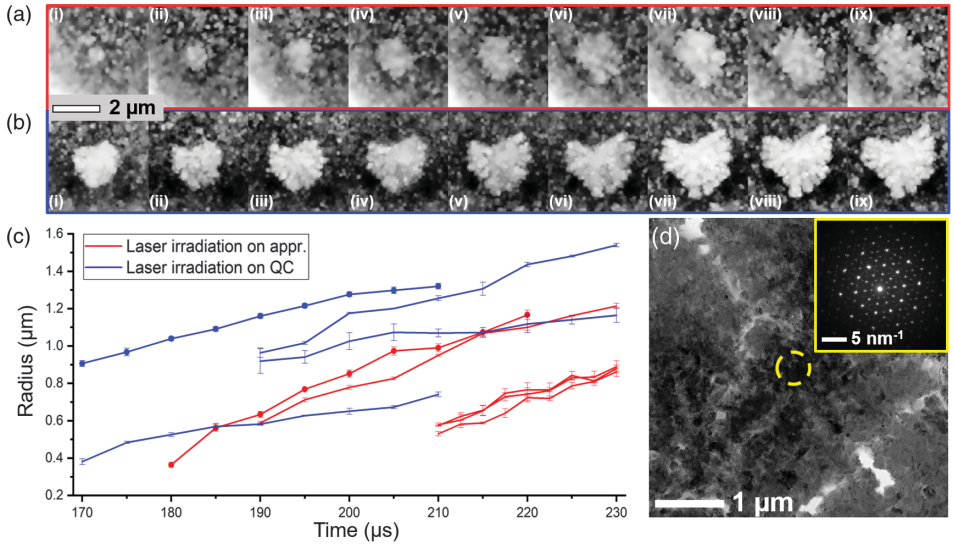

FIG. 2. Dynamics of QC precipitation following laser irradiation of Al-Cr thin film samples. Initial condition in (a) was the approximant phase $Al_{13}Cr_2$ and in (b) the Al-Cr icosahedral QC "seeds." In both cases, we focus on a single representative precipitate (in white). Time lapse between consecutive images is 5 μs. Note: the QC precipitate seen in (i) in (b) is not the same QC obtained in (ix) in (a). (c) Precipitate radius vs time, where 0 μs corresponds to the time at which the laser was fired. Equivalent radii were computed based on the area A covered by the growing QC phase (determined via image segmentation) and using the relationship $\sqrt{A/\pi}$. Data points corresponding to (a) and (b) are indicated with red and blue circles, respectively. Growth curves are compiled from multiple DTEM experiments. (d) TEM image of Al-Cr QC precipitate formed via laser irradiation. Inset shows a selected area diffraction pattern with a [000 001] zone axis taken from the highlighted area.

factors allow perturbations to grow in amplitude at the interphase boundary. Bearing these requirements in mind, the formation of dendritic structures upon solidification of a metallic liquid is relatively common due to the missing stabilizing effects against perturbations [46]. Conversely, the formation of solid-state dendrites is extremely rare in nature [44,46,47]. Nevertheless, the QC precipitates seen here uniquely satisfy all of these preconditions. For instance, past work shows that icosahedral QCs possess a nearly isotropic equilibrium Wulff shape [48] and that transition elements are slow diffusers in icosahedral QCs in comparison to the self-diffusion in Al [49]. Moreover, and as will be demonstrated below, 13-atom icosahedral motifs are common to both QC and approximant phases, thus satisfying precondition (iii). This should lead to a highly mobile interface between the two phases, as there are no kinetic limitations for atoms or clusters to incorporate into the growing QC.

In light of the above considerations, we can test the theoretical predictions of Mullins and Sekerka [50]. In their analysis, the critical precipitate radius $R_c(l)$ above which the lth-order spherical harmonic should grow is given as

$$R_c(l) = \frac{2[(1/2)(l+1)(l+2)+1]\gamma\Omega}{|(C_M - C_0)/C_0|\mathrm{RT}}, \qquad (1)$$

where γ is the interphase boundary energy, Ω is the molar volume, C_M is the initial solute composition in the supersaturated matrix; C_0 is the solute composition in the matrix in equilibrium with a precipitate having infinite radius, and RT is thermal energy. Because of a lack of data on the Al-Cr system, we used γ between Al-Mn icosahedral QC and the approximant Al_6Mn phase, 0.03 J/m^2 at 750 K [51,52] (note the Al-Mn quasicrystal is isostructural with the Al-Cr QC). Ω is 5.14×10^{-4} m^3/mol from the molecular weight of an $Al_{42}Cr_{13}$ Mackay cluster and the density of Al-Mn QC [53]. T, at which perturbations were observed in Fig. 2(a), is roughly 750 K (see also Fig. S1 in the Supplemental Material [34]). The values of $R_c(l)$ from the stability criterion of Eq. (1) are plotted in Fig. 3 against the relative supersaturation $|(C_M - C_0)/C_0|$, where we restrict l to be 6, 10, and 12. Only these values of l are possible under $l = 16$ given the 532 site group symmetry of the icosahedral QC phase [54].

In order to pinpoint where our DTEM experiment lands on this morphological stability diagram, we require estimates of the relative supersaturation $|(C_M - C_0)/C_0|$ and the critical radius R_c. We demonstrate in Fig. 2 that instabilities tend to grow at precipitate radii well below $R_c \simeq 2$ μm (see Fig. S4 in the Supplemental Material [34]). Likewise, we take the supersaturation to be its maximal value, i.e., $|(C_M - C_0)/C_0| \to 0.5$. As we show in Supplemental Material [34], this assumption is reasonable for the diffusion-limited growth of a spherical precipitate. In order to fit the experimental data to a model of the diffusion-limited growth, we needed an approximate measure of the diffusivity of Cr in the $Al_{13}Cr_2$ approximant matrix, which we determined through a thin film diffusion

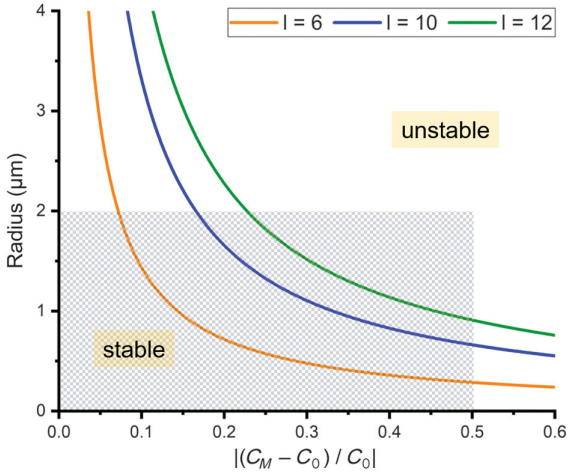

FIG. 3. Calculated critical precipitate radius $R_c(l)$ for relative stability as a function of supersaturation. Curves correspond to the lth-order spherical harmonic. Interface is radially stable below the neutral curve and radially unstable above it. Shaded area represents the conditions encountered in our DTEM experiment, the boundaries of which are determined by the maximum supersaturation and the average radius of the fully grown QCs.

experiment (see the Supplemental Material [34]). Our measurement of the supersaturation is an *upper bound* because it does not account for the diffusional interactions between neighboring QCs [55] [see condition (iv) above], nor does it account for defects that are created upon laser irradiation [56,57]. The shaded area in Fig. 3 indicates the region of the morphological stability diagram that we can access through our DTEM experiment. That all three $R_c(l)$ curves intersect this shaded region indicates that dendrites are indeed within the realm of experimental possibilities.

The reason that the QC can overcome the stabilizing influence of capillarity (surface tension) and form dendrites so readily is because of its structural similarity to the $Al_{13}Cr_2$ matrix [precondition (iii) above]. The unit cell of the approximant $Al_{13}Cr_2$ phase consists of three different types of 13-atom icosahedra, and these icosahedra are linked either by vertices, edges, or triangular faces or interlocked at the center of neighboring icosahedra [29,58]. Such icosahedral motifs are frequently observed in Al-Cr QCs as a substructure of 55-atom Mackay clusters [59]. The Mackay clusters are aligned with the fivefold axis of icosahedral QCs and produce a long-range icosahedral order [59]. Our MD simulations trace the emergence of the icosahedral motifs in $Al_{90}Cr_{10}$ alloys. According to Fig. 4 and Fig. S5 in the Supplemental Material [34], the dominant short-range order (SRO) in the quenched liquid $Al_{90}Cr_{10}$ is a 13-atom icosahedral cluster, as indicated by a low alignment score ($\sim$0.05) and hence a small deviation from the reference structure (the first coordination shell of a Mackay cluster). This can be attributed to the prevailing SRO in the liquid phase at high temperatures [60] (see Fig. S6 in the Supplemental Material [34]). We have also compared the Cr-centered structural motifs in the quenched alloy to the three types of icosahedra in the approximant $Al_{13}Cr_2$ phase (Fig. 4). Here, too, we observe a high degree of structural similarity despite the slight differences in Cr-Al bond lengths. Given the energetic stability of the icosahedral cluster, it stands to reason that the same motif will appear in solid phases of close compositions, such as the QC and the $Al_{13}Cr_2$ approximant. In light of these results, we suppose that the 13-atom icosahedral clusters can survive annealing and laser irradiation and ultimately contribute to the formation of icosahedral QCs in the solid state.

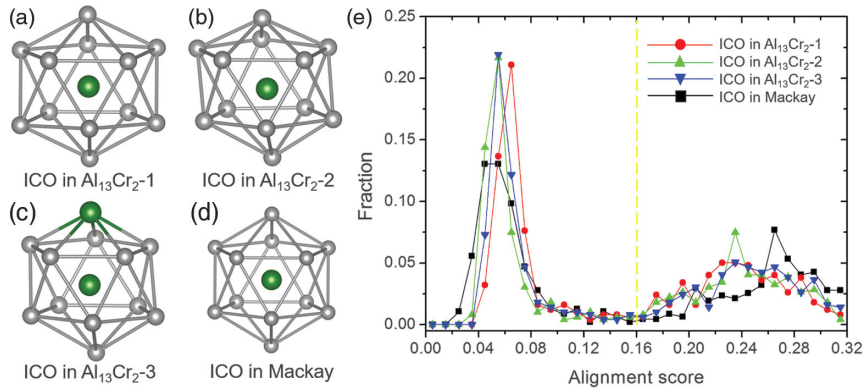

FIG. 4. SRO of $Al_{90}Cr_{10}$ alloy, quenched from 2200 to 700 K at a rate of 10^{11} K/s. For reference, we show (a)–(c) three types of 13-atom, Cr-centered clusters in the approximant $Al_{13}Cr_2$ phase and (d) a prototypical icosahedron (i.e., the first coordination shell of a 55-atom Mackay cluster). Note the simulated clusters depicted in (a)–(d) are slightly distorted from the referenced icosahedra. While they may look similar, they can be distinguished from each other: the corresponding ratio of average Cr-Al bond lengths in (a)–(d) is 1.03 : 1.02 : 1.01 : 1.00. The green and gray balls in (a)–(d) represent Cr and Al atoms, respectively. (e) Cluster analysis on rapidly quenched $Al_{90}Cr_{10}$ liquid, wherein the Cr-centered motifs are compared to those shown in (a)–(d). Clusters are said to have an SRO similar to the given template (or reference structure) when their alignment score is below the cutoff value of 0.16 (indicated by a yellow dashed line). Low alignment score indicates small structural deviation from the template. See the Supplemental Material [34] for further details.

The significance of these icosahedral clusters has long been a matter of debate in the scientific community. The central question is whether they impart a physical stability to QCs or if they simply appeal to our need to organize complex information into small units [61]. Here, we show that clusters are not only important from a *structural* perspective but also from a *kinetic* one: they facilitate the "easy" transition from one solid intermetallic phase to another. That is, the long-range icosahedral order in QCs can be readily obtained by the motion of a few atoms from the short-range icosahedral order in the approximant phase [62]. As the clusters move into registry, whether by local "matching" rules [63] or otherwise, they displace the surrounding Al atoms (solute rejection; see Fig. S3 in the Supplemental Material [34]). Clearly, this ordering occurs by a nucleation and growth mechanism (Fig. 2). Without this common structural motif between the QC and approximant phases, the interphase boundaries would possess a relatively low mobility, thereby *stabilizing* the precipitates against dendritic perturbations [64]. The existence of icosahedral clusters (Fig. 4) may also explain why we should see metastable QC precipitates in the first place and why QCs are often observed as intermediate phases in multistep nucleation processes [65]. These arguments can be extended to other phase transitions involving liquid or amorphous [66] precursors.

In summary, we have investigated the pulsed laser-induced growth of Al-Cr QC dendrites from an approximant phase. While QCs have been shown to grow dendritically in a *liquid* [67–69], we provide a real-time experimental assessment of this particular growth mode in the *solid state*. We rationalize the development of morphological instabilities based on the similarity in local orders between QC and approximant. With the aid of *ab initio* MD simulations, we trace this structural similarity to 13-atom, Cr-centered icosahedral clusters. These clusters readily assemble into icosahedral QCs without substantial rearrangements. This atomic picture fully explains the growth process of metastable QC dendrites in systems that are driven far from equilibrium.

We acknowledge support from the U.S. Department of Energy (DOE), Office of Science, Office of Basic Energy Sciences, under Award No. DE-SC0019118. Work at Lawrence Livermore National Laboratory (LLNL) was performed under the auspices of the U.S. DOE under Contract DE-AC52-07NA27344. Work at LLNL was supported by the Laboratory Directed Research and Development Program under project tracking code 18-SI-003. The research performed at the Ames Laboratory, which is operated for the U.S. DOE by Iowa State University, under contract No. DE-AC02-07CH11358 was funded by the U.S. DOE, Office of Science, Basic Energy Sciences, Materials Science and Engineering Division. We express our thanks to the Lurie Nanofabrication Center (LNF) at the University of Michigan for the LNF seed funding under Grant No. U066638 and David Sebastian from LNF for assisting in sample preparation. The authors acknowledge the Michigan Center for Materials Characterization $(MC)^2$ for use of the instruments and Dr. Kai Sun from $(MC)^2$ for fruitful discussions.

*Corresponding author.
shahani@umich.edu

[1] D. Shechtman, I. Blech, D. Gratias, and J. W. Cahn, Metallic Phase with Long-Range Orientational Order and No Translational Symmetry, Phys. Rev. Lett. **53**, 1951 (1984).
[2] A. I. Goldman and R. F. Kelton, Quasicrystals and crystalline approximants, Rev. Mod. Phys. **65**, 213 (1993).
[3] M. Quiquandon, A. Quivy, J. Devaud, F. Faudot, S. Lefebvre, M. Bessiere, and Y. Calvayrac, Quasicrystal and approximant structures in the al-cu-fe system, J. Phys. Condens. Matter **8**, 2487 (1996).
[4] I. Han, X. Xiao, H. Sun, and A. J. Shahani, A side-by-side comparison of the solidification dynamics of quasicrystalline and approximant phases in the Al–Co–Ni system, Acta Crystallogr. Sect. A **75**, 281 (2019).
[5] S. Lee, M. J. Bluemle, and F. S. Bates, Discovery of a frank-kasper σ phase in sphere-forming block copolymer melts, Science **330**, 349 (2010).
[6] C. R. Iacovella, A. S. Keys, and S. C. Glotzer, Self-assembly of soft-matter quasicrystals and their approximants, Proc. Natl. Acad. Sci. U.S.A. **108**, 20935 (2011).
[7] M. Engel, P. F. Damasceno, C. L. Phillips, and S. C. Glotzer, Computational self-assembly of a one-component icosahedral quasicrystal, Nat. Mater. **14**, 109 (2015).
[8] J. Schroers, D. Holland-Moritz, D. M. Herlach, and K. Urban, Growth kinetics of quasicrystalline and polytetrahedral phases of Al-Pd-Mn, Al-Co, and Al-Fe from the undercooled melt, Phys. Rev. B **61**, 14500 (2000).
[9] H. N. Thi, J. Gastaldi, T. Schenk, G. Reinhart, N. Mangelinck-Noel, V. Cristiglio, B. Billia, B. Grushko, J. Härtwig, H. Klein, and J. Baruchel, In situ and real-time probing of quasicrystal solidification dynamics by synchrotron imaging, Phys. Rev. E **74**, 031605 (2006).
[10] J. Gastaldi, G. Reinhart, H. Nguyen-Thi, N. Mangelinck-Noël, B. Billia, T. Schenk, J. Haertwig, B. Grushko, H. Klein, A. Buffet *et al.*, In situ study of quasicrystal growth by synchrotron x-ray imaging, Philos. Mag. **87**, 3079 (2007).
[11] I. Han, X. Xiao, and A. J. Shahani, Probing the growth and melting pathways of a decagonal quasicrystal in real-time, Sci. Rep. **7**, 17407 (2017).
[12] N. Senabulya, X. Xiao, I. Han, and A. J. Shahani, On the kinetic and equilibrium shapes of icosahedral $Al_{71}Pd_{19}Mn_{10}$ quasicrystals, Scr. Mater. **146**, 218 (2018).
[13] R. A. Dunlap and K. Dini, Structure and stability of quasicrystalline aluminium transition-metal alloys, J. Phys. F **16**, 11 (1986).
[14] R. A. Dunlap, G. Stroink, K. Dini, and D. F. Jones, Structural, electrical and magnetic properties of icosahedral Al-Co alloys, J. Phys. F **16**, 1247 (1986).

[15] J. A. Knapp and D. M. Follstaedt, Measurements of Melting Temperatures of Quasicrystalline Al-Mn Phases, Phys. Rev. Lett. **58**, 2454 (1987).

[16] K. Hiraga, E. Abe, and Y. Matsuo, The structure of an Al-Pd decagonal quasicrystal studied by high-resolution electron microscopy, Philos. Mag. Lett. **70**, 163 (1994).

[17] T. LaGrange, M. R. Armstrong, K. Boyden, C. G. Brown, G. H. Campbell, J. D. Colvin, W. J. DeHope, A. M. Frank, D. J. Gibson, F. V. Hartemann *et al.*, Single-shot dynamic transmission electron microscopy, Appl. Phys. Lett. **89**, 044105 (2006).

[18] T. LaGrange, G. H. Campbell, B. W. Reed, M. Taheri, J. B. Pesavento, J. S. Kim, and N. D. Browning, Nanosecond time-resolved investigations using the *in situ* of dynamic transmission electron microscope (dtem), Ultramicroscopy **108**, 1441 (2008).

[19] T. LaGrange, B. W. Reed, and D. J. Masiel, Movie-mode dynamic electron microscopy, MRS Bull. **40**, 22 (2015).

[20] T. LaGrange, B. W. Reed, M. K. Santala, J. T. McKeown, A. Kulovits, J. M. K. Wiezorek, L. Nikolova, F. Rosei, B. J. Siwick, and G. H. Campbell, Approaches for ultrafast imaging of transient materials processes in the transmission electron microscope, Micron **43**, 1108 (2012).

[21] J. T. McKeown, A. K. Kulovits, C. Liu, K. Zweiacker, B. W. Reed, T. LaGrange, J. M. K. Wiezorek, and G. H. Campbell, In situ transmission electron microscopy of crystal growth-mode transitions during rapid solidification of a hypoeutectic Al–Cu alloy, Acta Mater. **65**, 56 (2014).

[22] J. T. McKeown, Y. Wu, J. D. Fowlkes, P. D. Rack, and G. H. Campbell, Simultaneous in-situ synthesis and characterization of Co@ Cu core-shell nanoparticle arrays, Adv. Mater. **27**, 1060 (2015).

[23] J. T. McKeown, K. Zweiacker, C. Liu, D. R. Coughlin, A. J. Clarke, J. K. Baldwin, J. W. Gibbs, J. D. Roehling, S. D. Imhoff, P. J. Gibbs *et al.*, Time-resolved *in situ* measurements during rapid alloy solidification: Experimental insight for additive manufacturing, JOM **68**, 985 (2016).

[24] K. Zweiacker, J. T. McKeown, C. Liu, T. LaGrange, B. W. Reed, G. H. Campbell, and J. M. K. Wiezorek, Determination of crystal growth rates during rapid solidification of polycrystalline aluminum by nano-scale spatio-temporal resolution in situ transmission electron microscopy, J. Appl. Phys. **120**, 055106 (2016).

[25] T. Pinomaa, J. M. McKeown, J. M. K. Wiezorek, N. Provatas, A. Laukkanen, and T. Suhonen, Phase field modeling of rapid resolidification of Al-Cu thin films, J. Cryst. Growth **532**, 125418 (2020).

[26] E. Abe and A. P. Tsai, Structure of a metastable al3ni decagonal quasicrystal: Comparison with a highly perfect $Al_{72}Ni_{20}Co_8$, J. Alloys Compd. **342**, 96 (2002).

[27] K. Nagao, T. Inuzuka, K. Nishimoto, and K. Edagawa, Experimental Observation of Quasicrystal Growth, Phys. Rev. Lett. **115**, 075501 (2015).

[28] M. Newville, Ifeffit: Interactive xafs analysis and feff fitting, J. Synchrotron Radiat. **8**, 322 (2001).

[29] E. Liotti, C. A. Kirk, I. Todd, K. S. Knight, and S. C. Hogg, Synchrotron x-ray and neutron investigation of the structure and thermal expansion of the monoclinic $Al_{13}Cr_2$ phase, J. Alloys Compd. **781**, 1198 (2019).

[30] L. Zhang, J. Han, H. Wang, R. Car, and E. Weinan, Deep Potential Molecular Dynamics: A Scalable Model with the Accuracy of Quantum Mechanics, Phys. Rev. Lett. **120**, 143001 (2018).

[31] L. Zhang, J. Han, H. Wang, W. Saidi, R. Car, and E. Weinan, End-to-end symmetry preserving inter-atomic potential energy model for finite and extended systems, in *32nd Conference on Neural Information Processing Systems (NeurIPS 2018), Montréal, Canada* (2018), pp. 4436–4446.

[32] H. Wang, L. Zhang, J. Han, and E. Weinan, Deepmd-kit: A deep learning package for many-body potential energy representation and molecular dynamics, Comput. Phys. Commun. **228**, 178 (2018).

[33] X. W. Fang, C. Z. Wang, Y. X. Yao, Z. J. Ding, and K. M. Ho, Atomistic cluster alignment method for local order mining in liquids and glasses, Phys. Rev. B **82**, 184204 (2010).

[34] See Supplemental Material, which includes Refs. [33,35–39], at http://link.aps.org/supplemental/10.1103/PhysRevLett.125.195503 for more details about our ab initio molecular dynamics simulations.

[35] G. Kresse and J. Furthmüller, Efficiency of ab-initio total energy calculations for metals and semiconductors using a plane-wave basis set, Comput. Mater. Sci. **6**, 15 (1996).

[36] G. Kresse and J. Furthmüller, Efficient iterative schemes for ab initio total-energy calculations using a plane-wave basis set, Phys. Rev. B **54**, 11169 (1996).

[37] S. Plimpton, Fast parallel algorithms for short-range molecular dynamics, J. Comput. Phys. **117**, 1 (1995).

[38] S. Nosé, A unified formulation of the constant temperature molecular dynamics methods, J. Chem. Phys. **81**, 511 (1984).

[39] W. G. Hoover, Canonical dynamics: Equilibrium phase-space distributions, Phys. Rev. A **31**, 1695 (1985).

[40] A. Sadoc, P. Lagarde, and P. Sainfort, Exafs study of icosahedral Al Cr, Int. J. Mod. Phys. B **1**, 133 (1987).

[41] A. L. Pope and T. M. Tritt, Thermal conductivity of quasicrystalline materials, in *Thermal Conductivity* (Springer, New York, 2004), pp. 255–259.

[42] W. M. Haynes, *CRC Handbook of Chemistry and Physics* (CRC press, Boca Raton, 2014).

[43] J. W. Gibbs, D. Tourret, P. J. Gibbs, S. D. Imhoff, M. J. Gibbs, B. A. Walker, K. Fezzaa, and A. J. Clarke, In situ x-ray observations of dendritic fragmentation during directional solidification of a Sn-Bi alloy, JOM **68**, 170 (2016).

[44] P. G. Shewmon, Interfacial stability in solid-solid transformations, Trans. Metall. Soc. AIME **233**, 736 1965.

[45] M. J. Aziz and W. J. Boettinger, On the transition from short-range diffusion-limited to collision-limited growth in alloy solidification, Acta Metall. Mater. **42**, 527 (1994).

[46] R. D. Doherty, Role of interfaces in kinetics of internal shape changes, Met. Sci. **16**, 1 (1982).

[47] R. A. Ricks, A. J. Porter, and R. C. Ecob, The growth of γ precipitates in nickel-base superalloys, Acta Metall. **31**, 43 (1983).

[48] C. Beeli and H.-U. Nissen, Growth morphology of icosahedral Al–Mn–Pd single quasicrystals, Philos. Mag. B **68**, 487 (1993).

[49] H.-R. Trebin, *Quasicrystals: Structure and Physical Properties* (John Wiley & Sons, New York, 2003).
[50] W. W. Mullins and R. F. Sekerka, Morphological stability of a particle growing by diffusion or heat flow, J. Appl. Phys. **34**, 323 (1963).
[51] K. F. Kelton and J. C. Holzer, Crystallization of the al mn icosahedral phase, Mater. Sci. Eng. **99**, 389 (1988).
[52] L. Battezzati, C. Antonione, and F. Marino, Some thermodynamic and kinetic aspects of icosahedral phase nucleation in Al-Mn, J. Mater. Sci. **24**, 2324 (1989).
[53] K. Kimura, T. Hashimoto, K. Suzuki, K. Nagayama, H. Ino, and S. Takeuchi, Structure and stability of quasicrystalline Al–Mn alloys, J. Phys. Soc. Jpn. **55**, 534 (1986).
[54] L. Elcoro, J. M. Perez-Mato, and G. Madariaga, Systematic structure refinement of quasicrystals using symmetry-adapted parameters, J. Non-Cryst. Solids **153**, 155 (1993).
[55] N. Senabulya and A. J. Shahani, Growth interactions between icosahedral quasicrystals, Phys. Rev. Mater. **3**, 093403 (2019).
[56] D. A. Lilienfeld, M. Nastasi, H. H. Johnson, D. G. Ast, and J. W. Mayer, Amorphous-to-Quasicrystalline Transformation in the Solid State, Phys. Rev. Lett. **55**, 1587 (1985).
[57] D. A. Lilienfeld, M. Nastasi, H. H. Johnson, D. G. Ast, and J. W. Mayer, The quasicrystalline transformation in the AlCr system, J. Mater. Res. **1**, 237 (1986).
[58] M. Audier, M. Durand-Charre, E. Laclau, and H. Klein, Phase equilibria in the Al Cr system, J. Alloys Compd. **220**, 225 (1995).
[59] K. H. Kuo, Mackay, anti-Mackay, double-Mackay, pseudo-Mackay, and related icosahedral shell clusters, Structural chemistry **13**, 221 (2002).
[60] P. Ganesh and M. Widom, Signature of nearly icosahedral structures in liquid and supercooled liquid copper, Phys. Rev. B **74**, 134205 (2006).
[61] P. A. Thiel, Quasicrystal surfaces, Annu. Rev. Phys. Chem. **59**, 129 (2008).
[62] V. Elser, Comment on "Quasicrystals: A New Class of Ordered Structures", Phys. Rev. Lett. **54**, 1730 (1985).
[63] J. E. S. Socolar and P. J. Steinhardt, Quasicrystals. II. Unit-cell configurations, Phys. Rev. B **34**, 617 (1986).
[64] A. A. Chernov, *Modern Crystallography III: Crystal Growth* (Springer Science & Business Media, New York, 2012), Vol. 36.
[65] G. Kurtuldu, K. F. Shamlaye, and J. F. Löffler, Metastable quasicrystal-induced nucleation in a bulk glass-forming liquid, Proc. Natl. Acad. Sci. U.S.A. **115**, 6123 (2018).
[66] G. G. Long, Karena W. Chapman, P. J. Chupas, L. A. Bendersky, L. E. Levine, F. Mompiou, J. K. Stalick, and J. W. Cahn, Highly Ordered Noncrystalline Metallic Phase, Phys. Rev. Lett. **111**, 015502 (2013).
[67] V. T. Swamy, S. Ranganathan, and K. Chattopadhyay, Rapidly solidified Al–Cr alloys: Crystalline and quasicrystalline phases, J. Mater. Res. **4**, 539 (1989).
[68] A. Singh and S. Ranganathan, Quasicrystalline and crystalline phases and their twins in rapidly solidified Al Mn Fe alloys, J. Non-Cryst. Solids **153**, 86 (1993).
[69] F. Schurack, J. Eckert, and L. Schultz, Synthesis and mechanical properties of cast quasicrystal-reinforced Al-alloys, Acta Mater. **49**, 1351 (2001).